Aralia elata leaf extracts synthetize ZnO based nanoclusters and its dye removal applications

Jin Huang

1218005300@qq.com

Northeast Forestry University

zhiguo Liu

Northeast Forestry University

yujie Fu

Beijing Forestry University

xiuhua Zhao

Northeast Forestry University

Article

Keywords: NCs: Nanoclusters, AE: Aralia elata, ZnO: Zinc oxide, ZnONCs: Zinc oxide nanoclusters , AE-ZnONCs: Aralia elata- zinc oxide nanoclusters, MB: Methylene blue, SY: Sunset yellow

Posted Date: March 10th, 2026

DOI: https://doi.org/10.21203/rs.3.rs-9054863/v1

Additional Declarations: No competing interests reported.

Version of Record: A version of this preprint was published at Scientific Reports on May 1st, 2026. See the published version at https://doi.org/10.1038/s41598-026-51235-1.

Aralia elata leaf extracts synthetize ZnO based nanoclusters and its dye removal applications

Jin Huang[1,2,3,4], Zhiguo Liu[1,2,3,4], Yujie Fu[5] , Xiuhua Zhao[1,2,3,4]*

1 College of Chemistry, Chemical Engineering and Resource Utilization, Key Laboratory of Forest Plant Ecology Ministry of Education, Northeast Forestry University, Harbin 150040, China

2 Heilongjiang Provincial Key Laboratory of Ecological Utilization of Forestry-based Active Substances, Harbin 150040, China

3 National Engineering Laboratory of Bio-Resource Eco-Utilization, Harbin 150040, China

4 Concept Validation Center for Green Extraction and Formulation Technology of Forest Food and Drug Active Substances in Heilongjiang Province

5 School of Biological Sciences and Technology, Beijing Forestry University, Beijing, 100091, China.

*Corresponding author E-mail: xiuhuazhao@nefu.edu.cn

Keywords: zinc oxide nanoclusters, *Aralia elata*, green synthesis, plant extracts, dye removal

Abstract

At the nanoscale, various materials exhibit significant changes in their electrical and optical properties, showing optical and electrical performance that is entirely different from that of macroscopic materials, and thus have been widely applied. Among them, zinc oxide nanoclusters (ZnONCs) are commonly applied in the fields of antibacterial and bacteriostatic, photocatalysis, ultraviolet shielding, sensor preparation, and dye removal. In this paper, to reduce the use of toxic and harmful chemical reagents, the leaf extract of *Aralia elata* was used as the chemical modifier and stabilizer, and the functionalized zinc oxide nanocluster material (AE-ZnONCs) was prepared by the green hydrothermal synthesis method, which can be used for the removal of organic dyes in wastewater. SEM confirmed that the surface of AE-ZNONCs was a loose lamellar structure, with AE extract adhering to the material surface. TEM characterization shows that the internal structure of AE-ZnONCs is a loose lamellar structure. EDS and XRD confirmed that the nanomaterials contained zinc oxide and AE plant components. TGA characterization confirmed that the mass proportion of AE extract attached to the material surface was 18.3%. AE-ZnONCs could rapidly and efficiently adsorb methylene blue (MB) and sunset yellow (SY) dyes from water, with the adsorption process following second-order kinetics and adhering to the Freundlich-type multilayer adsorption isotherm model. The green hydrothermal preparation method for functionalized zinc oxide boasts advantages such as abundant raw materials, high cost-effectiveness, environmental friendliness, controllable parameters, simple equipment, and easy operation, with broad application prospects.

Abbreviations

NCs: Nanoclusters

AE: *Aralia elata*

ZnO: Zinc oxide

ZnONCs: Zinc oxide nanoclusters

AE- ZnONCs: *Aralia elata*- zinc oxide nanoclusters

MB: Methylene blue

SY: Sunset yellow

1. Introduction

Nanomaterials, owing to their unique optical, mechanical, and electromagnetic properties, are currently widely applied across diverse fields including medicine, materials industry, chemical engineering, and catalyst materials[1-3]. Commonly encountered nanomaterials include ZnO, Ag, Au, and Pt, amongst which ZnO nanomaterials exhibit antibacterial properties, ultraviolet absorption, dye adsorption, and photocatalytic efficacy[4, 5]. In the preparation methods of nanomaterials, ball milling (physical method) and sol-gel (chemical method) are currently predominant[6, 7]; however, ball milling tends to cause dust pollution, and chemical methods often involve the use of toxic and harmful reagents, resulting in irreversible environmental pollution. To improve these processes, this paper adopts the green hydrothermal method, which belongs to the green chemical synthesis and preparation methods. Green hydrothermal synthesis typically involves creating a local high-temperature and high-pressure environment in a sealed container by artificially adjusting external heating temperature, system pH value, and other parameters, thereby synthesizing, preparing, and modifying functionalized nanomaterials in a relatively short period of time[8, 9]. The advantages of this method include: fast reaction rate, predominantly aqueous reaction system, mild reaction conditions, high cost-effectiveness of the process, no introduction of impurities, and environmental friendliness. Nanometer-sized ZnO materials exhibit significant application value in various fields such as chemical engineering and medicine. Future research focuses will continue to be on optimizing and enhancing the comprehensive performance of materials and optimizing green and friendly preparation processes[10, 11].

In the green hydrothermal synthesis process for preparing nanomaterials, natural plant extracts are commonly used as reaction reagents. By wholly or partially replacing toxic and harmful chemical reducing agents, stabilizers, and modifiers, the damage and pollution to the environment are minimized to the greatest extent[12, 13]. In specific synthesis reactions, organic compounds such as polysaccharides, alkaloids, organic acids, flavonoids, polyphenols, and terpenoids contained in plant extracts provide groups such as carboxyl, hydroxyl, and amino groups, which promote the uniform growth of ZnO nanomaterials through chelation. Due to the differences in active ingredients contained in different types of plants, the morphology and internal structure of the synthesized ZnO also vary[14]. Aida et al. used hexamethylenetetramine as a slow precipitant for $ZnCl_2$ and modified the synthesized nano-ZnO materials using *Hibiscus* and *Artemisia* plant extracts, respectively. Experimental results showed that different types of plant extracts control the uniform and non-uniform growth processes by altering the properties of the solution. The *Hibiscus* extract has a lower viscosity, resulting in a predominance of uniform ZnO precipitation.

In contrast, the *Artemisia* extract has a higher viscosity, leading to a predominance of non-

uniform ZnO precipitation[15]. Kurbanova et al. used $Zn(NO_3)_2$, $AgNO_3$, and *Juniperus* plant extracts as raw materials to prepare Ag-modified ZnO nanomaterials with a mushroom-like appearance. The preparation conditions did not require thermal treatment or adjustment of the solution pH value. These materials exhibited potent antibacterial activity against Staphylococcus aureus and Escherichia coli and can be used as a sustainable antimicrobial agent in medical and environmental fields[16]. *Aralia elata*, a common wild plant in the Northern Hemisphere, contains multiple active ingredients such as polysaccharides, saponins, polyphenols, and flavonoids in its leaf extracts, which can serve as stabilizers and modifiers for nanomaterials. Functionalized nano-zinc oxide materials (AE-ZnONCs) are synthesized under hydrothermal conditions. The preparation of functional nanomaterials also demonstrates the multi-level and high-value utilization of wild plant resources.

In various production processes in the industrial sector, synthetic dyes have advantages over natural dyes in terms of color variety, dyeing efficiency, physicochemical stability, and price, thus gaining widespread application. Among them, methylene blue (cationic species dye) and sunset yellow (anionic species dye) are common organic pollutants in water bodies and are widely used in multiple fields[17, 18]. The extensive use of organic dyes has caused significant pollution and damage to water bodies and the environment. How to quickly remove dyes from water bodies has gradually become a research hotspot. Currently, methods for removing organic dyes from water bodies mainly include physical co-precipitation, biological microorganisms, and chemical adsorption. The operation process using the nanomaterial adsorption method is relatively simple, has a wide range of applicability, and achieves remarkable results[19, 20]. The functionalized nanomaterial AE-ZnONCs prepared in this paper have dye removal efficacy, and their synthesis method is simple, green, and environmentally friendly, possessing particular research value and significance.

2. Materials and methods

2.1. Materials

Aralia elata leaves were purchased from Yichun, Heilongjiang Province. The zinc sulfate heptahydrate, methylene blue (MB), sunset yellow (SY), and sodium hydroxide were purchased from Sinopharm Group (analytical grade). The Milli-Q water (Electrical resistivity$\geqslant$18.2MΩ·cm) was self-made in the laboratory.

2.2. AE-ZnONCs synthesis steps

2.2.1. Synthesis on AE leaf extracts

The leaves of *Aralia elata* were washed, dried, and crushed to obtain AE solid samples. Mix AE powder and an appropriate volume of Milli-Q water evenly in a glass beaker and ultrasonically treat for 30 min. Then, heat and extract for 30 min at a water temperature of 75℃ and a stirring rate of 500 r/min. The extracted mixture was filtered and centrifuged to retain the supernatant, and then diluted with an appropriate amount of Milli-Q water to obtain 5% AE leaf extract.

2.2.2 Synthesis of ZnO NCs

Mix 5mL of AE leaf extract (5%) with 20mL of Milli-Q water in a beaker and stir for 20 min at a stirring speed of 400 r/min. Slowly add 5 mL of $ZnSO_4$ (1%), then add a small amount of 1mol/L NaOH solution to adjust the pH of the mixed solution to 8.0, and continue to stir for 30 min. The

mixed solution was transferred to the polytetrafluoroethylene high-pressure tank reactor, and the reactor was heated in an oven with the heating temperature set at 140℃. After the reaction, the AE-ZnONCs mixed suspension was obtained. To optimize the reaction conditions, the heating times were set at 1h, 2h, 3h, 4h, and 5h. The optimal heating duration was determined by the surface morphology and structure to be characterized. The suspension of AE-ZnONCs was centrifuged for 30 min (rotational speed 8000 r/min). The precipitated part was washed three times with Milli-Q water, and the precipitate was dried in an oven at 40 °C to obtain the solid sample of AE-ZnONCs.Figure 1 shows the synthesis steps for the preparation of AE-ZnONCs colloid. The AE leaf aqueous extract is light-green in color, while the AE-ZnONCs colloidal solution exhibits earthy yellow-green.

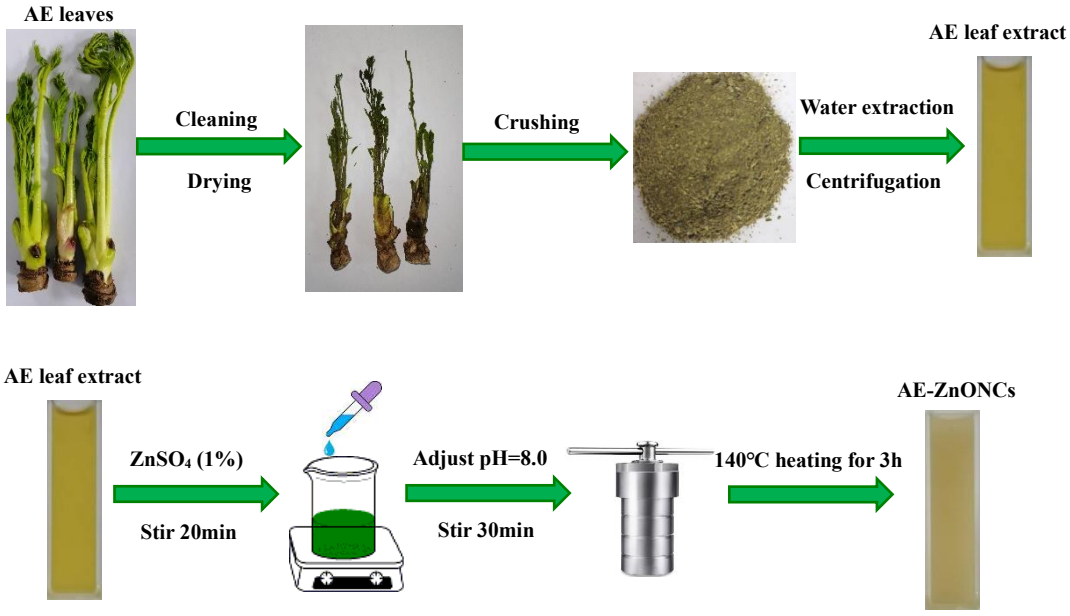

Figure 1. The synthesis steps of the AE leaf extract and AE-ZnONCs colloid

2.3. AE-ZnO NCs characterization

2.3.1. Scanning electron microscope and energy dispersive spectroscopy (SEM and EDS)

The morphology and structure of AE-ZnONCs solids heated for 1 to 5 hours were characterized by scanning electron microscopy, and the optimal synthesis process was determined based on the morphological and structural characteristics. The 50 mg AE-ZnONCs sample was fixed on both sides of the sample stage with conductive carbon-based materials, and Pt metal was sputtered on its surface using a metal sputtering instrument. The processed samples were placed in the sample chamber of the electron microscope. The morphology and structure of the samples were observed under an acceleration voltage of 10kV and an appropriate current. The elemental composition and content were identified by an energy scattering spectrometer. According to the SEM characterization results, the heating duration of the nanomaterials was determined. (Instrument model: Thermofisher Apreo 2c)

2.3.2. Ultraviolet-visible absorption spectroscopy (UV-vis)

The liquid samples of AE-ZnONCs were tested and characterized using a ultraviolet-visible spectrophotometer. An appropriate amount of AE-ZnONCs colloidal solution was ultrasonically treated, diluted with a proper amount of Milli-Q water, shaken well, and the UV-vis absorption spectra were scanned in the full wavelength range of 200nm to 800nm. (Instrument model: Persee TU-1901)

2.3.3. Transmission electron microscopy (TEM)

The transmission structure of AE-ZnONCs colloid samples was characterized by transmission electron microscopy. After ultrasonic treatment of AE-ZnONCs suspension for 15 min, 100μL to 300μL of AE-ZnONCs colloidal solution was dropped onto a carbon alloy mesh. After natural drying, the TEM test was conducted, with an acceleration voltage set at 200kV. (Instrument model: JEOL JEM-F200)

2.3.4. X-ray diffraction (XRD)

X-ray diffraction instruments identified AE leaf and AE-ZnONCs solid samples. The crystal structure and its component characteristics were determined by analyzing the diffraction angle and the corresponding relative intensity. Approximately 500mg of the sample was laid flat and compacted in the bracket. Set the scanning mode to continuous scanning in the instrument, with a step width of 0.01°, scanning speed of 20°/min, high voltage potential of 40 kV, current of 30 mA, X-ray wavelength of 0.1540593 nm, and record experimental data within the range of 4° ~ 90°(Instrument model: Rigaku SmartLab-SE). Based on the XRD characterization results, in this paper, the Scherrer formula was used to calculate the size of the crystal particles. The Scherrer equation: $D=k \cdot \lambda/(\beta \cdot \cos\theta)$. D: crystallite size (nm); k: Scherrer constant; λ: X-ray wavelength (Å), β: Half-width of diffraction peak(rad); θ: Bragg angle in degrees (deg)[21, 22].

2.3.5. Fourier transform infrared spectroscopy (FTIR)

The Fourier Transform infrared spectrometer characterized the FTIR spectrum of AE-ZnONCs. Grind 300mg of dry spectral pure grade KBr and 3mg of the solid sample (AE leaf/ AE-ZnONCs) evenly in a mortar. Weigh 80mg of the mixture and press it into a tablet. Prepare the sample under pressure at 20MPa for 1 min. Taking the spectral pure grade KBr salt plate as the blank control, with the FTIR scanning resolution of 1 cm^{-1}, the data within the wavenumber range of 400 cm^{-1} ~ 4000 cm^{-1} were recorded. (Instrument model: Thermo Nicolet-IS10)

2.3.6. Thermogravimetric analysis (TGA)

TGA, DSC, and DTG data curves characterize the thermogravimetric properties of materials. 5mg to 15mg of the dried sample(AE leaf/ AE-ZnONCs materials) were placed in an alumina crucible. The N_2 is used as the protective gas (flow rate 20mL/min). The heating process ranges from 40 ℃ to 800 ℃, with a heating rate of 10 °C/min. Record the data curves of TGA, DSC, and DTG of the samples. (Instrument model: Netzsch STA449-F3)

2.3.7. Dye removal kinetics experiment

Based on dynamic experiments, this paper investigates the efficacy of functionalized nanomaterials (AE-ZnONCs) colloid in removing methylene blue (MB) and sunset yellow (SY) dyes.

160 mL of AE-ZnONCs colloidal solution with 40 mL of MB (10mg/L) / SY (30mg/L) solution were mixed under room temperature (25℃), dark conditions, and 600r/min stirring speed. The reaction times were: 0, 1, 2, 5, 10, 20, 30, 40, 50, 60, 600 min. It was confirmed that complete adsorption was achieved after 600 min in multiple experiments. When the set reaction time was reached, extract 8mL of the mixed solution and centrifuge it at 8000r/min for 20min. Measure the absorbance value of MB dye at λ=665 nm and the absorbance value of SY dye at λ=485 nm using a UV-visible spectrophotometer. Calculate the dye removal rate and draw the dye removal kinetics curve. Blank controls were made using AE-ZnONCs colloidal solution and distilled water (volume ratio 4:1). Dye removal rate (%) =$[(C_0-C_1)/C_0]\times100\%$ (where C_0: initial dye concentration mg/L; C_1: post-reaction dye concentration mg/L).

The adsorption kinetic models on organic dyes by AE-ZnONCs can be fitted by pseudo-first-order or pseudo-second-order formulas[23]. The following formulas exhibit the two adsorption kinetic models. The Pseudo-first-order model formula: $\ln (Qe - Qt) = \ln Qe - k_1 \cdot t$; The Pseudo-second-order model formula: $t/Qt = 1/(k_2 \cdot Q_e^2) + t / Q_e$.

Note: Q_e: The adsorption capacity in equilibrium state; Q_t: The adsorption capacity at the adsorption time t; k_1: The rate constant of pseudo-first-order; t: The adsorption time; k_2: The rate constant of pseudo-second-order. This article calculates the dynamic fitting curve based on experimental results, calculates the fitting equation, and studies its adsorption principle.

2.3.8. Dye removal isotherm experiment

Based on isothermal experiments, this paper studies the efficacy of functionalized nanomaterial (AE-ZnONCs) colloids in the removal of methylene blue (MB) and sunset yellow (SY) dyes. Six copies of AE-ZnONCs (8.0mL) samples were mixed separately with 2.0 mL solutions of dyes (MB/SY) at concentrations of 5, 10, 15, 20, 25, and 30 mg/L. The reaction temperature was set at 25℃, and the mixture was stirred in a dark shaking incubator for 600min. After reaching the adsorption equilibrium, the supernatant was collected by centrifugation, and the remaining dye concentration was measured. Blank controls were made using AE-ZnONCs colloidal solution and distilled water (volume ratio 4:1).

The isotherm kinetic models on organic dyes by AE-ZnONCs can be fitted by the Langmuir or the Freundlich formulas[24]. The following formulas exhibited the two isotherm kinetic models.
The Langmuir isotherm model formula: $C_e/Q_e = 1/(Q_{max} \cdot K_L) + C_e/Q_{max}$; The Freundlich isotherm model formula: $\mathrm{Ln}(Q_e) = \mathrm{Ln}(K_f) + 1/n \cdot \mathrm{Ln}(C_e)$.

Note: Q_e: The adsorption capacity in equilibrium state; Q_{max}: The maximum adsorption capacity; k_L: The Langmuir constant related to adsorption capacity; k_f: The constant related to adsorption; n: The parameter related to adsorption strength or surface heterogeneity. This article calculates the isotherm fitting curve based on experimental results, calculates the fitting equation, and studies its adsorption principle.

3. Experimental characterization and discussion

3.1. SEM and EDS characterization

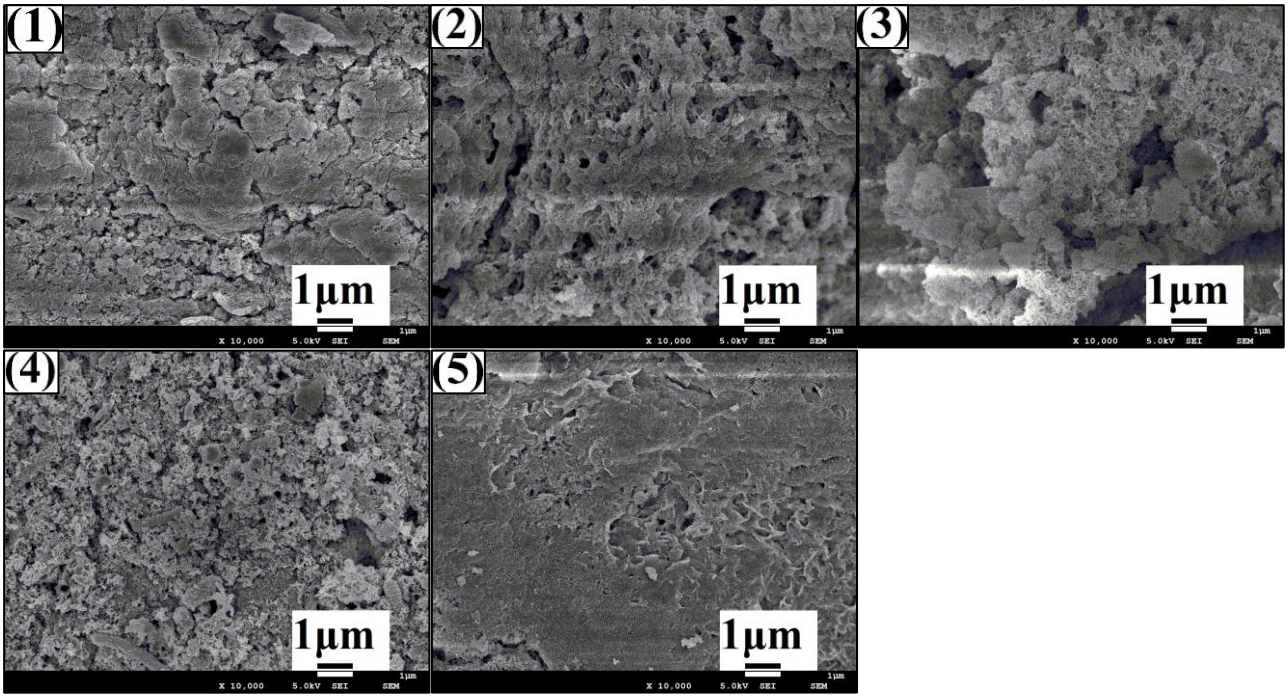

Figure 2. SEM characterization results of AE-ZnONCs samples with different heating durations (Magnified 10,000 times, Figures 1~5 represent heating durations of 1 h~5 h)

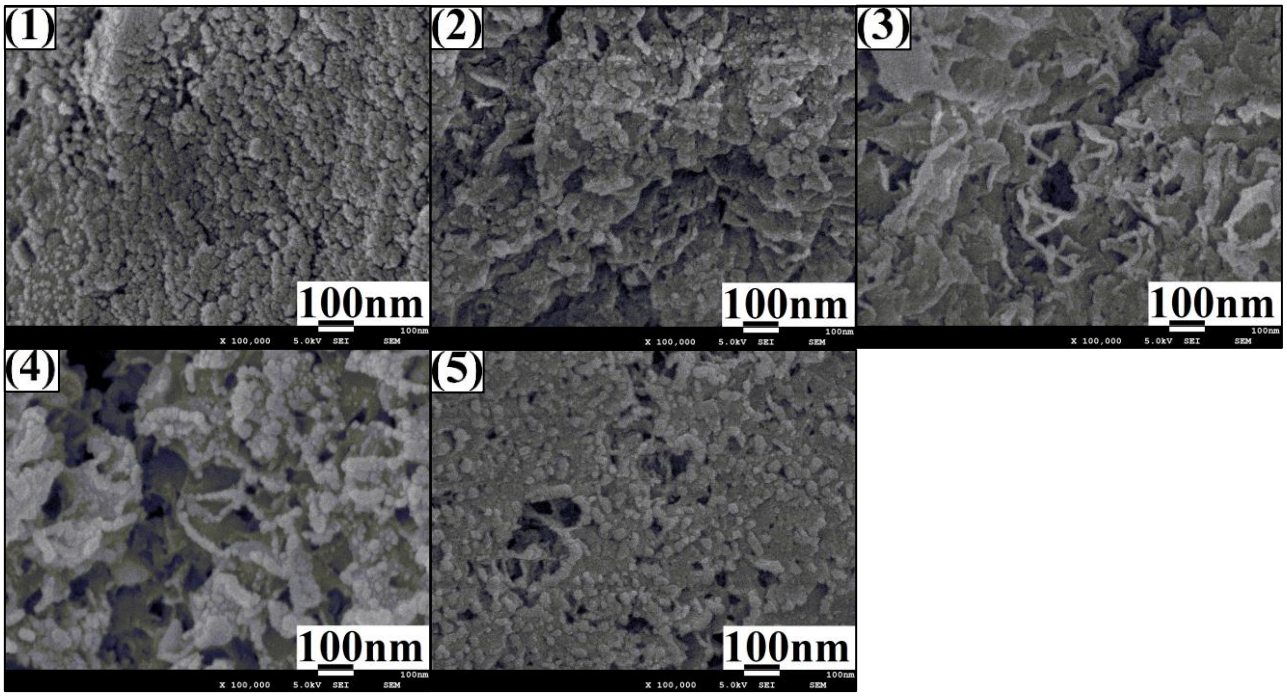

Figure 3. SEM characterization results of AE-ZnONCs samples with different heating durations (Magnified 100,000 times, figures 1~5 represent heating durations of 1 h~5 h)

Figure 2 is a 10000 magnified photo of the AE-ZnONCs sample; Figure 3 is a 100000 magnified photo of the AE-ZnONCs sample; Figure 4 shows the EDS characterization results of AE-ZnONCs samples (heated for 4h). From the characterization results of the five samples with heating durations ranging from 1h ~ 5h, it can be concluded that as the heating time extends from 1 h ~ 4 h, the functionalized AE-ZnONCs gradually change from the amorphous precipitate state to the polygonal layered morphology. As the heating time continued to expand, the lamellar structure of the sample heated for 5h gradually transformed into a compacted, contracted, and agglomerated state, and no longer had a high relative surface area[25].

It can be seen from Figure 3 that the extract of AE leaves adheres to the surface of the lamellar material. Powder materials usually experience agglomeration during high-temperature processing, which is typically classified into soft agglomeration and hard agglomeration. Soft agglomeration results from van der Waals forces and electrostatic attraction, and these forces are relatively weak. Hard agglomeration results from the reconstruction of the internal structure of the crystal under high-temperature conditions, transforming from an amorphous state to a regularly arranged crystal form, generating covalent bonds, and making the forces more robust. After being heated, the inner lining of the reaction vessel generates a specific high-pressure environment, gradually transforming the amorphous $Zn(OH)_2$ produced in the aqueous reaction into closely arranged ZnONCs with a lamellar structure[26].

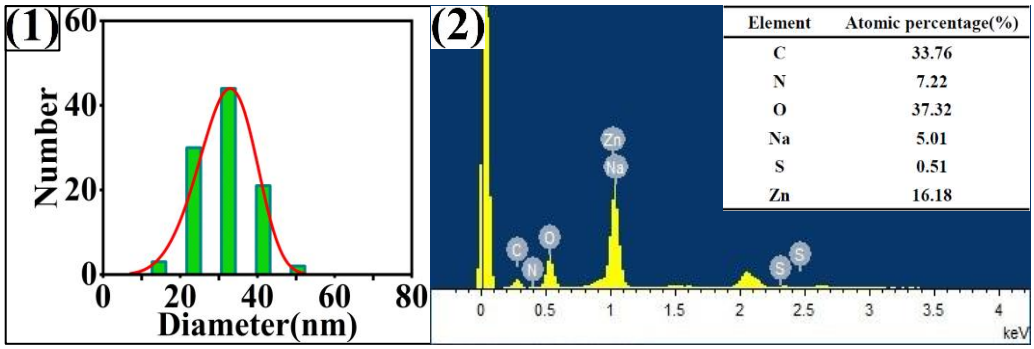

Figure 4. Particle size distribution, EDS characterization, and elemental atomic ratio results of AE-ZnONCs sample (heating duration 4h)

(1) Particle size distribution graph of the sample; (2) EDS characterization and atomic ratio of elements

Figure 4 shows the particle size distribution, EDS characterization, and elemental atomic ratio results of the AE-ZnONCs sample heated for 4 hours. From Figure 4-1, it can be seen that the average particle size of AE-ZnONCs is 31.71nm (with the maximum particle size of 52.73nm and the minimum particle size of 14.16nm). In Figure 4-2, the EDS characterization reveals that the nanomaterial sample contains C, N, O, Na, S, and Zn elements, with Zn accounting for 16.18% of the atomic ratio. The Na and S elements may originate from Na^+ and SO_4^{2-} carried during the precipitation process in the solution. The C, N, and O elements are derived from plant extracts[27].

3.2. Ultraviolet-visible spectra characterization

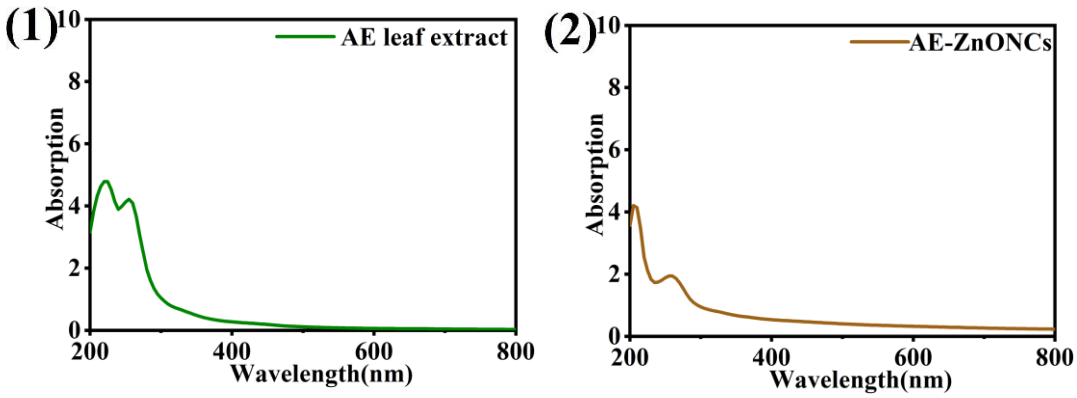

Figure 5. Ultraviolet-visible characterization results (1) AE leaf extract; (2) AE-ZnONCs colloid

Figure 5 presents the UV-Vis spectral absorption characterization results of the AE leaf extract solution and AE-ZnONCs. As shown in the figure, AE-ZnONCs exhibit absorption in the 200 nm~350 nm UV region but show no significant absorption peaks in the 400 nm~800 nm range. The absorption curve of AE-ZnONCs resembles that of the AE leaf extract solution[28]. After high-pressure hydrothermal reaction in the autoclave, while generating flake-like ZnONCs solids, some active substances from the AE leaf extract were retained.

3.3. TEM characterization

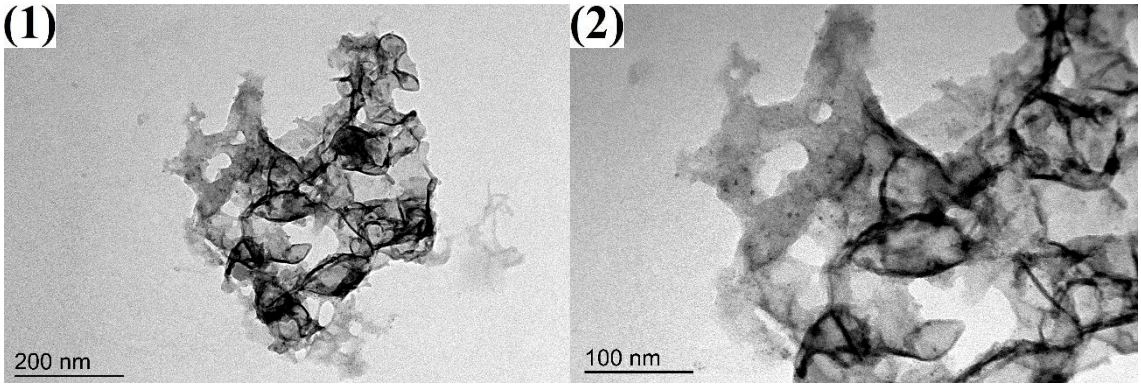

Figure 6. TEM characterization results of AE-ZnONCs colloid

(1) AE-ZnONCs scale of 200 nm; (2) AE-ZnONCs scale of 100 nm

Figure 6 presents the TEM characterization results of the AE-ZnONCs colloidal solution. From the figure, it can be seen that the internal morphological structure of the AE-ZnONCs colloid is an irregular layered shape with some agglomeration features, which is consistent with the SEM surface morphology characterization results. All the images are bright-field scanning results. The dark parts represent polygonal stacked zinc oxide; the light parts represent the AE leaf extract[29]. The AE extract is attached to the surface of ZnONCs and has a specific chemical modification effect.

3.4. XRD characterization

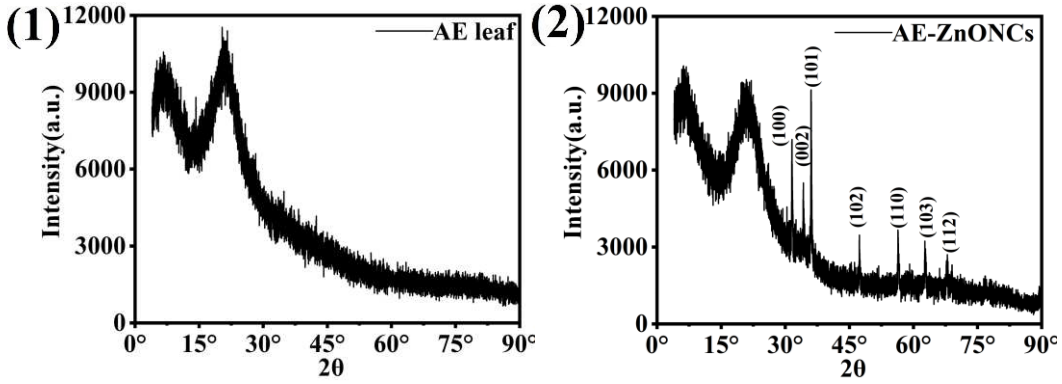

Figure 7. XRD characterization results of AE leaf powder and AE-ZnONCs powder

(1) AE leaf powder; (2) AE-ZnONCs powder

Figure 7 shows the XRD test characterization results of AE leaf powder and AE-ZnONCs. In Figure 7-1, the diffraction pattern of the AE leaf extract shows a broad diffraction peak near 20°, confirming that its internal structure is amorphous. The XRD characterization results in Figure 7-2 still contain the broad diffraction peaks shown in Figure 7-1, confirming that the AE leaf extract has a specific structural modification effect on the surface structure of functionalized nanomaterials. In Figure 7-2, the characteristic diffraction peaks of ZnO are located at 31.6°,34.2°, 36.0°, 47.4°, 56.4°, 62.7°, and 67.9°. Corresponding to the five structural planes of ZnO cubic crystals (100),(002),(101),(102),(110),(103), and (112) (JCPDS serial number 36-1451), which confirmed that under the conditions of closed high pressure, high temperature, and appropriate heating duration, AE-ZnONCs has a stable crystal structure[30].

The Scherrer formula was used to calculate crystallite size: $D=k \cdot \lambda/(\beta \cdot \cos\theta)$. Note: D: photocatalyst material crystallite size (nm); k: shape factor; λ: the X-rays wavelength (Å), β: Full width at half maximum; θ: Bragg angle in degrees (°) [31, 32].

Based on the XRD diffraction peak results (Figure 7-2), the average size of functionalized ZnONCs was calculated to be 35.85nm using the Scherrer formula, which is consistent with the SEM morphological characterization results (31.71nm). Appropriate heating duration facilitates the formation of dense and compact layered structures[33, 34]; Polysaccharides in the AE leaf extract serve as stabilizers and modifiers, resulting in a solution with high overall viscosity, which tends to produce heterogeneous and relatively smaller-sized ZnONCs[35].

3.5. FTIR characterization

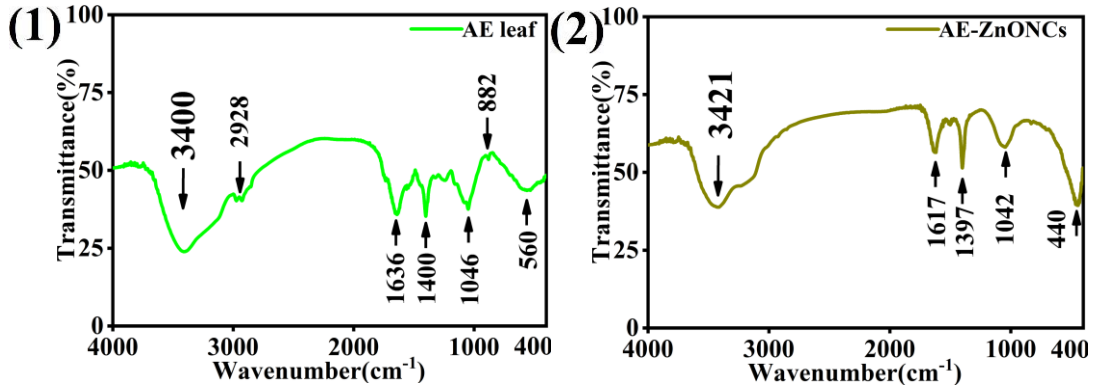

Figure 8. FTIR spectrum characterization results

(1)AE leaf powder; (2) AE-ZnONCs powder

Figure 8 shows the infrared spectral characterization results of AE leaf powder and AE-ZnONCs. In the figure 8-1, the broad peak at 3400 cm^{-1} represents the stretching vibration of a large number of -OH groups within the polysaccharide molecules in the AE leaf extract; The 2928 cm^{-1} absorption peak is derived from the extension and contraction vibration of the C-H bond within the polysaccharide molecule. 1636 cm^{-1} and 1400 cm^{-1} represent the asymmetric and symmetric stretching vibrations of the carboxyl group $-COO^-$. Vibrations of 1046 cm^{-1} and 882cm^{-1} represent the six-membered polysaccharide carbon skeleton of C-O-C[36], confirming that the surface layer of the functionalized nanomaterial AE-ZnONCs is attached with components of AE leaf extract. A peak of 560 cm^{-1} represents the bending vibration of the C-C=O bond between aldehydes and ketones. The infrared absorption at 440nm is composed of inorganic ZnO[37]. In figure 8-2, the functionalized nanomaterials basically maintain some peak shapes of the raw materials of the AE leaf extract. However, due to a specific interaction between ZnONCs material and AE leaf extract, the FTIR peak shapes of -OH and $-COO^-$ are partially shifted.

3.6. TGA characterization

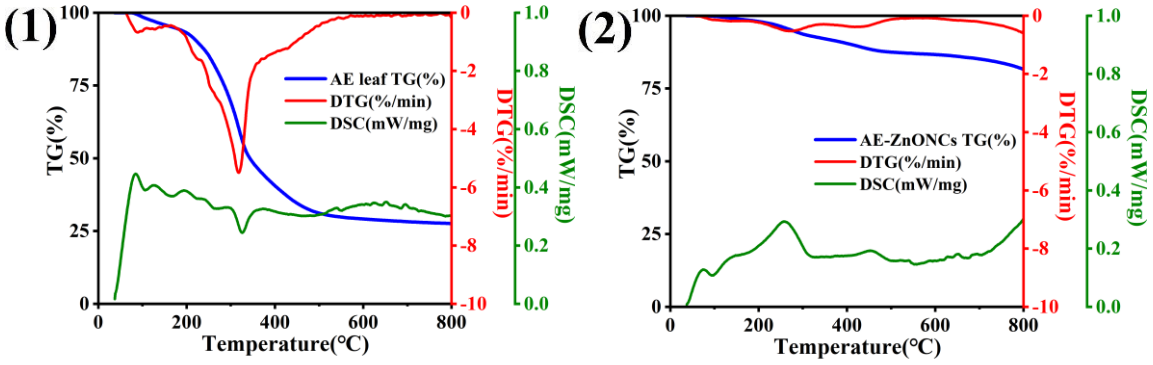

Figure 9. TGA/DTG/DSC characterization on AE leaf and AE-NPs powder

(1) AE leaf powder; (2) AE-ZnONCs powder

Figure 9 presents the TGA/DTG/DSC characterization curves of AE leaf and AE-ZnONCs powder. Overall, both samples exhibit the most tremendous mass loss between 200°C ~ 500°C, with the 200°C ~ 350°C range corresponding to the cleavage of polysaccharide glycosidic bonds and the

350°C ~ 500°C range indicating the deep decomposition of the polysaccharide carbon-hydrogen skeleton[38]. The AE leaf extract shows adhesion to the functionalized material.

The main component of AE leaves is insoluble cellulose, which belongs to the polysaccharide compound category; the extract of AE leaves primarily consists of soluble polysaccharides, saponins, and acidic substances. As shown in figure 9-1, the mass of the AE leaf sample in the TG curve decreases from 100% to 27.6%, resulting in a mass loss of 72.4%. At point 320°C, the AE leaf sample exhibits rapid mass loss, accompanied by a peak in the DTG curve. The DSC curve overall confirms that the decomposition of AE leaves is an endothermic process. From figure 9-2, the mass of the AE-ZnONCs sample in the TG curve decreases from 100% to 81.7%, with a mass loss of 18.3%. When the temperature reaches 280°C, the TG curve shows the fastest mass reduction, while peaks appear in both the DTG and DSC curves. The DSC curve overall confirms that the decomposition of AE-ZnONCs material is an endothermic process, as the decomposition of surface-adsorbed AE leaf extract requires heat absorption[39].

3.7. Dye removal kinetics results

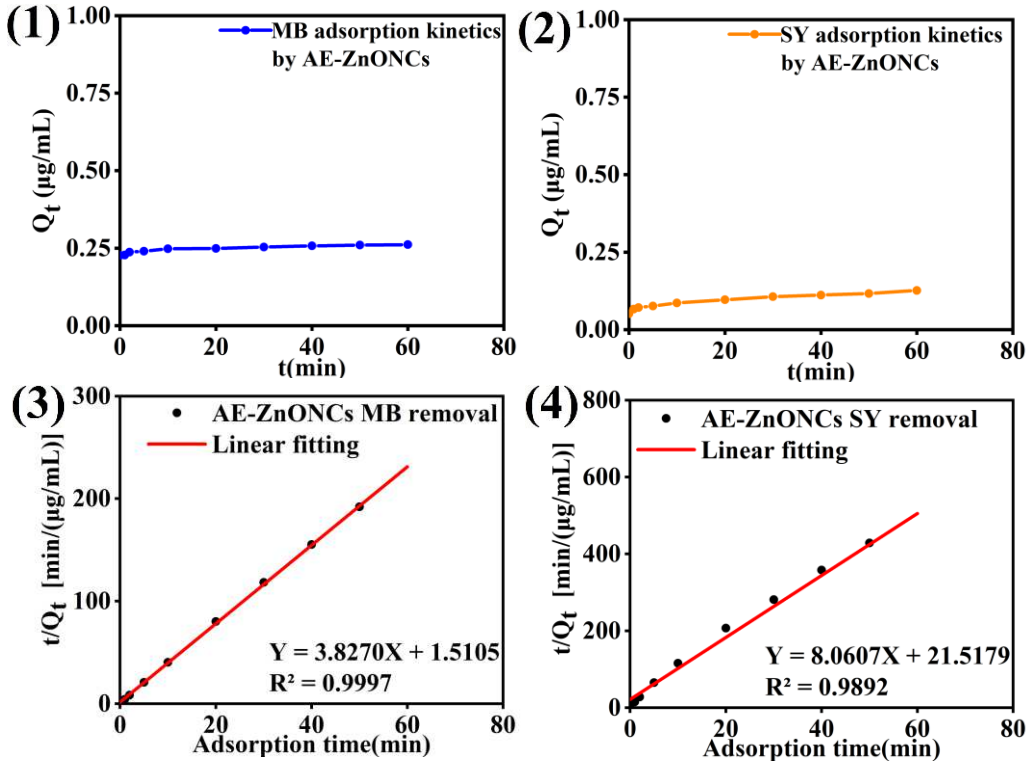

Figure 10. Experimental results on dye removal kinetics

(1) The MB adsorption capacity by AE-ZnONCs; (2) The SY adsorption capacity by AE-ZnONCs; (3) The MB t/Qt-t linear fitting by AE-ZnONCs; (4) The SY t/Qt-t linear fitting by AE-ZnONCs

Table 1. Summary of kinetic model fitting parameters for AE-ZnONCs adsorption of MB and SY dyes

Types of dyes	Pseudo-first-order model			Pseudo-second-order model		
	K_1(min^{-1})	Q_e(μg·mL^{-1})	R^2	K_2(mL·μg·min^{-1})	Q_e(μg·mL^{-1})	R^2
MB	0.0118	0.0576	0.899	9.70	0.261	0.999
SY	0.0222	0.0819	0.974	3.02	0.124	0.989

Figure 10 showed the AE-ZnONCs experimental results of dye removal kinetics. From Figure 10, it can be known that the adsorption capacity of AE-ZnONCs for dye MB is approximately 0.25 μg/mL, and for dye SY, it is approximately 0.15 μg/mL. The adsorption process rapidly increases within 5 min and is basically completed within 20 min. As time goes on, the increase in adsorption capacity becomes less significant, and the adsorption reaction rate first increases quickly and then slows down. Table 1 summarizes the kinetic model fitting parameters for the adsorption of MB and SY dyes by AE-ZnONCs. From the table, it can be seen that based on the fitted R^2 value, the adsorption process follows second-order kinetics, with chemical adsorption playing a dominant role. Meanwhile, experiments demonstrate that AE-ZnONCs exhibit excellent and rapid adsorption for both cationic dyes (MB) and anionic dyes (SY)[40].

3.8. Dye removal isotherm results

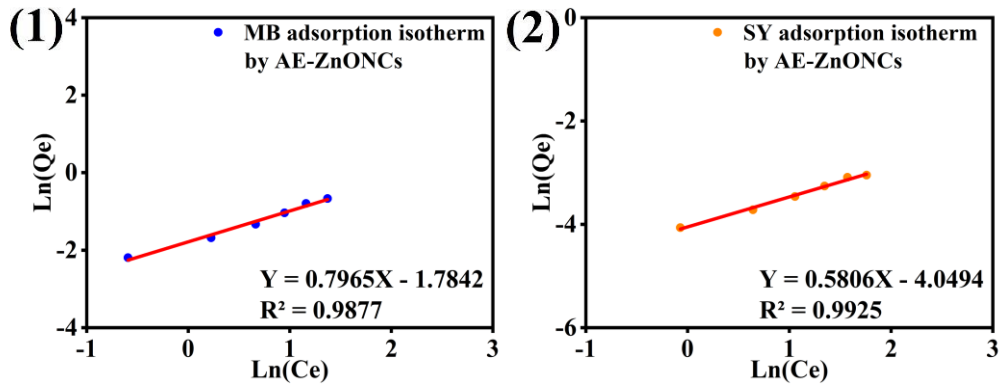

Figure 11. Experimental results on dye removal isotherms
(1)MB adsorption isotherm by AE-ZnONCs; (2) SY adsorption isotherm by AE-ZnONCs

Table 2. Summary of fitting parameters for the isotherm model of AE-ZnONCs adsorbing MB and SY dyes

Types of dyes	Langmuir			Freundlich		
	Q_{max}(mg·L^{-1})	K_L(L·mg^{-1})	R^2	n	K_f(mg·L^{-1})	R^2
MB	1.590	0.116	0.650	1.26	0.168	0.988
SY	0.0792	0.255	0.952	1.72	0.0174	0.993

Figure 11 showed the AE-ZnONCs experimental results for the dye removal isotherms. Table 2 is a summary table of the fitting parameters for the isotherm model of AE-ZnONCs adsorbing MB and SY dyes. From figure 11 and table 2, it can be seen that based on the fitted R^2 value, the Freundlich model can better fit the adsorption process of AE-ZnONCs for MB and SY dyes. The isotherm adsorption process belongs to the Freundlich adsorption process, which is a heterogeneous, multilayer adsorption process characterized by surface inhomogeneity and intermolecular interactions[41, 42].

3.9. Summary on dyes removal mechanisms

Figure 12 showed a schematic diagram of the removal mechanism of the AE-ZnONCs colloidal material. The functionalized nanoscale AE-ZnONCs material synthesized in this study exhibits a polygonal lamellar structure, providing abundant adsorption sites. The AE leaf extract contains compounds such as polysaccharides, flavonoids, and polyphenols, which also supply functional

groups like -COOH and -OH to adsorb dye molecules. The adsorption mechanism of functionalized nanocomposites for MB and SY dyes in water can be attributed to multiple mechanisms, including electrostatic attraction, hydrogen bonding, and van der Waals forces[43]. The dye removal experiments conducted in this study were carried out under light-avoidance conditions[44]. Rapid stirring facilitates the dispersion of AE-ZnONCs and their binding with MB and SY dye molecules, enabling swift adsorption of the dyes and achieving the goal of water purification.

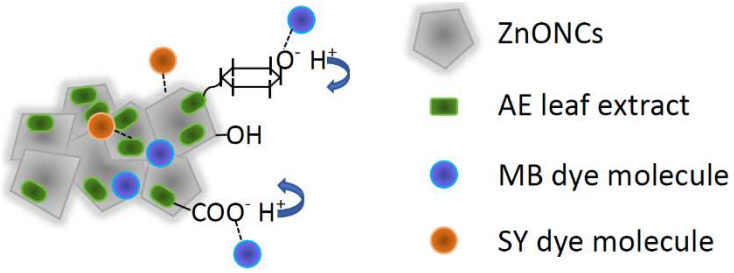

Figure 12. The diagrams on the mechanism for MB and SY dye removal by AE-ZnONCs.

4. Conclusions

This study successfully prepared functionalized AE-ZnONCs materials using *Aralia elata* leaf extract as a stabilizer and modifier through a green hydrothermal method. The green hydrothermal synthesis process offers advantages such as simple workflow, environmental friendliness, high cost-effectiveness, and energy-saving and emission-reduction capabilities. SEM characterization of the material's surface structure confirmed that 4h was the optimal heating time; The average particle size of the ZnONCs material is 31.71nm. TEM verified the loose layered structure of AE-ZnONCs; The characterization results of EDS, XRD, and TGA confirmed that the material contains ZnO and AE leaf extract components. Dye removal experiments demonstrated the material's efficacy in rapidly eliminating organic dyes like methylene blue (MB) and sunset yellow (SY) in aquatic environments. The adsorption process of AE ZnONCs colloids towards MB and SY dyes belongs to second-order kinetics (chemical adsorption process), and the isotherm adsorption process is more in line with the Friedrich model. The application of AE leaf extract in modifying functionalized nanomaterials contributes to the high-value utilization of wild plant resources. Future research will further optimize material performance and green preparation processes.

Data availability statement

In this research, all data that supported the findings were included in the article.

Funding

The authors gratefully acknowledge: financial support from the research project:
(1)Extraction, separation, structural modification, and mechanism of action of characteristic flavonoids from forest sources (ZKJB231700004)
(2)The Regional cooperation project on technological support for high-quality development of the large agricultural economy in Altay, Xinjiang (ZZDYF241700001)

Competing interests

The authors declared that they had no competing interests.

References

1. Boles, M. A., Ling, D., Hyeon, T. & Talapin, D. V. (2016) The surface science of nanocrystals. *Nature Materials* **15(2)**:141-153.
2. Zhao, Q. R., Wang, S. S., Lv, Z. P., Zupanic, A., Guo, S. X., Zhao, Q. Y., Jiang, L. & Yu, Y. D. (2022) Using nanomaterials to increase the efficiency of chemical production in microbial cell factories: A comprehensive review. *Biotechnology Advances* **59**:16.
3. Kumar, R., Kumar, P., Gupta, S., Paliwal, G., Kumar, M. & Singh, M. (2024) A Review on Advancements in Nanomaterial Synthesis, Characterization, and Applications: Towards Sustainable and Innovative Solutions. *Brazilian Journal of Physics* **54(4)**:13.
4. Sampath, S., Bhushan, M., Saxena, V., Pandey, L. M. & Singh, L. R. (2022) Green synthesis of Ag doped ZnO nanoparticles: study of their structural, optical, thermal and antibacterial properties. *Materials Technology* **37(13)**:2785-2794.
5. Mishra, P. K., Mishra, H., Ekielski, A., Talegaonkar, S. & Vaidya, B. (2017) Zinc oxide nanoparticles: a promising nanomaterial for biomedical applications. *Drug Discovery Today* **22(12)**:1825-1834.
6. Aga, K. W., Efa, M. T. & Beyene, T. T. (2022) Effects of Sulfur Doping and Temperature on the Energy Bandgap of ZnO Nanoparticles and Their Antibacterial Activities. *Acs Omega* **7(12)**:10796-10803.
7. Hu, Y. F., Li, B. L., Yu, C. L., Fang, H. C. & Li, Z. S. (2023) Mechanochemical preparation of single atom catalysts for versatile catalytic applications: A perspective review. *Materials Today* **63**:288-312.
8. Goncalves, R. A., Toledo, R. P., Joshi, N. & Berengue, O. M. (2021) Green Synthesis and Applications of ZnO and TiO2 Nanostructures. *Molecules* **26(8)**:2236.
9. Yang, G. & Park, S. J. (2019) Conventional and Microwave Hydrothermal Synthesis and Application of Functional Materials: A Review. *Materials* **12(7)**:18.
10. Hossain, M. Z., Nayem, S. M. A., Alam, M. S., Islam, M. I., Seong, G. & Chowdhury, A. (2025) Hydrothermal ZnO Nanomaterials: Tailored Properties and Infinite Possibilities. *Nanomaterials* **15(8)**:32.
11. Chauhan, A. K., Kataria, N. & Garg, V. K. (2020) Green fabrication of ZnO nanoparticles using Eucalyptus spp. leaves extract and their application in wastewater remediation.

Chemosphere **247**:14.

12. Greeshma, K. P. & Thamizselvi, R. (2023) Phytogenic synthesis of ZnO nanoparticles from Catharanthus Roseus and Morinda Citrifolia leaf extract and its promising multifunctional biological applications. *Journal of Drug Delivery Science and Technology* **87**:11.
13. Tesfaye, M., Gonfa, Y., Tadesse, G., Temesgen, T. & Periyasamy, S. (2023) Green synthesis of silver nanoparticles using Vernonia amygdalina plant extract and its antimicrobial activities. *Heliyon* **9(6)**:14.
14. Mardosaite, R., Jurkeviciute, A. & Rackauskas, S. (2021) Superhydrophobic ZnO Nanowires: Wettability Mechanisms and Functional Applications. *Crystal Growth & Design* **21(8)**:4765-4779.
15. Aida, M. S., Alonizan, N., Zarrad, B. & Hjiri, M. (2023) Influence of plant extract on the homogeneous and heterogeneous green chemistry synthesis of nanostructured ZnO. *Journal of Taibah University for Science* **17(1)**:7.
16. Kurbanova, Z., Pereira, S. I. A., Sousa, A. S. S., Piccirillo, C., Shaislamov, U., Yubuta, K., Teshima, K., Eitinger, T. & Hojamberdiev, M. (2025) Juniperus pseudosabina extract-mediated green synthesis of zinc oxide artichoke-like structures for antibacterial applications. *Journal of Cleaner Production* **514**:13.
17. Repon, M. R., Dev, B., Rahman, M. A., Jurkoniene, S., Haji, A., Alim, M. A. & Kumpikaite, E. (2024) Textile dyeing using natural mordants and dyes: a review. *Environmental Chemistry Letters* **22(3)**:1473-1520.
18. Pizzicato, B., Pacifico, S., Cayuela, D., Mijas, G. & Riba-Moliner, M. (2023) Advancements in Sustainable Natural Dyes for Textile Applications: A Review. *Molecules* **28(16)**:22.
19. Yaqoob, A. A., Parveen, T., Umar, K. & Ibrahim, M. N. M. (2020) Role of Nanomaterials in the Treatment of Wastewater: A Review. *Water* **12(2)**:30.
20. Tan, K. B., Vakili, M., Hord, B. A., Poh, P. E., Abdullah, A. Z. & Salamatinia, B. (2015) Adsorption of dyes by nanomaterials: Recent developments and adsorption mechanisms. *Separation and Purification Technology* **150**:229-242.
21. Rabiei, M., Palevicius, A., Monshi, A., Nasiri, S., Vilkauskas, A. & Janusas, G. (2020) Comparing Methods for Calculating Nano Crystal Size of Natural Hydroxyapatite Using X-Ray Diffraction. *Nanomaterials* **10(9)**:21.
22. Xie, Y. B. & Yuan, C. W. (2003) Visible-light responsive cerium ion modified titania sol and nanocrystallites for X-3B dye photodegradation. *Applied Catalysis B-Environmental* **46(2)**:251-259.
23. Das, C., Sen, S., Singh, T., Ghosh, T., Paul, S. S., Kim, T. W., Jeon, S., Maiti, D. K., Im, J. & Biswas, G. (2020) Green Synthesis, Characterization and Application of Natural Product Coated Magnetite Nanoparticles for Wastewater Treatment. *Nanomaterials* **10(8)**:1615.
24. Ge, R. X., Wang, J. J., Piao, J. L., Pan, Z. H., Zhang, Z. H., Yang, Y. T., Huang, J. & Liu, Z. G. (2025) Green Synthesis of Sodium Alginate/Casein Gel Beads and Applications. *Nanomaterials* **15(6)**:18.
25. Sun, P. P., Lv, Z. B. & Sun, C. J. (2024) Study on the Synthesis of Nano Zinc Oxide Particles under Supercritical Hydrothermal Conditions. *Nanomaterials* **14(10)**:19.
26. Mutukwa, D., Taziwa, R. & Khotseng, L. E. (2022) A Review of the Green Synthesis of ZnO Nanoparticles Utilising Southern African Indigenous Medicinal Plants. *Nanomaterials* **12(19)**:22.

27. Mahlaule-Glory, L. M., Mbita, Z., Ntsendwana, B., Mathipa, M. M., Mketo, N. & Hintsho-Mbita, N. C. (2019) ZnO nanoparticles via Sutherlandia frutescens plant extract: physical and biological properties. *Materials Research Express* **6(8)**:14.
28. Wang, Y. Q., Yang, J., Kong, J. H., Jia, H. X. & Yu, M. H. (2015) ZnO microspheres: Controllable preparation and optical properties. *Superlattices and Microstructures* **86**:228-235.
29. Kolodziejczak-Radzimska, A. & Jesionowski, T. (2014) Zinc Oxide-From Synthesis to Application: A Review. *Materials* **7(4)**:2833-2881.
30. Thilagavathi, T. & Geetha, D. (2013) Low-temperature hydrothermal synthesis and characterization of ZnO nanoparticles. *Indian Journal of Physics* **87(8)**:747-750.
31. Hassanzadeh-Tabrizi, S. A. (2023) Precise calculation of crystallite size of nanomaterials: A review. *Journal of Alloys and Compounds* **968**:20.
32. Logeswari, P., Silambarasan, S. & Abraham, J. (2015) Synthesis of silver nanoparticles using plants extract and analysis of their antimicrobial property. *Journal of Saudi Chemical Society* **19(3)**:311-317.
33. Rawat, K. & Goyal, M. (2022) Effect of size, shape, orientation, pressure and temperature on elastic properties of nanomaterials. *High Temperatures-High Pressures* **51(2)**:109-128.
34. Goyal, M. & Goyal, V. (2021) Effect of size and temperature on vacancy concentration in nanomaterials. *Pramana-Journal of Physics* **95(3)**.
35. Zheng, Y. Y., Monty, J. & Linhardt, R. J. (2015) Polysaccharide-based nanocomposites and their applications. *Carbohydrate Research* **405**:23-32.
36. Das, C., Singh, S., Bhakta, S., Mishra, P. & Biswas, G. (2022) Bio-modified magnetic nanoparticles with Terminalia arjuna bark extract for the removal of methylene blue and lead (II) from simulated wastewater. *Chemosphere* **291(2)**:132673.
37. Begum, S. N. & Kumuthini, R. (2023) Characterization of zinc oxide nano particles synthesized via chemical and green method. *Journal of Ovonic Research* **19(5)**:505-512.
38. Mohammed, J. K., Mahdi, A. A., Ahmed, M. I., Ma, M. J. & Wang, H. X. (2020) Preparation, deproteinization, characterization, and antioxidant activity of polysaccharide from Medemia argun fruit. *International Journal of Biological Macromolecules* **155**:919-926.
39. Mohammadi-Aloucheh, R., Habibi-Yangjeh, A., Bayrami, A., Latifi-Navid, S. & Asadi, A. (2018) Enhanced anti-bacterial activities of ZnO nanoparticles and ZnO/CuO nanocomposites synthesized using Vaccinium arctostaphylos L. fruit extract. *Artificial Cells Nanomedicine and Biotechnology* **46**:S1200-S1209.
40. Nerkar, N. V., Kondawar, S. B., Brahme, S. K. & Kim, Y. H. (2018) Polyaniline/ZnO nanocomposites for the removal of methyl orange dye from waste water. *International Journal of Modern Physics B* **32(19)**:5.
41. Srivastava, V. & Choubey, A. K. (2019) Kinetic and isothermal study of effect of transition metal doping on adsorptive property of zinc oxide nanoparticles synthesized via green route using Moringa oleifera leaf extract. *Materials Research Express* **6(12)**:12.
42. Praipipat, P., Ngamsurach, P., Srirat, P. & Chaiphumee, P. (2024) Engineered biosorbents of pomelo (Citrus maxima (Burm.f.) Merr) peels modified with zinc oxide and titanium dioxide for methylene blue dye sorption. *Scientific Reports* **14(1)**:19.
43. Reghioua, A., Barkat, D., Jawad, A. H., Abdulhameed, A. S., Rangabhashiyam, S., Khan, M. R. & Alothman, Z. A. (2021) Magnetic Chitosan-Glutaraldehyde/Zinc Oxide/Fe3O4 Nanocomposite: Optimization and Adsorptive Mechanism of Remazol Brilliant Blue R Dye

Removal. *Journal of Polymers and the Environment* **29(12)**:3932-3947.

44. Nayak, A., Sahoo, J. K., Sahoo, S. K. & Sahu, D. (2022) Removal of congo red dye from aqueous solution using zinc oxide nanoparticles synthesised from Ocimum sanctum (Tulsi leaf): a green approach. *International Journal of Environmental Analytical Chemistry* **102(19)**:7889-7910.